Condition Monitoring and Fault Diagnosis of Permanent Magnet Synchronous Motor Stator Winding Using the Continuous Wavelet Transform and Machine Learning

Research paper

Przemysław Pietrzak[ID], Marcin Wolkiewicz*[ID]

Wrocław University of Science and Technology, 50-370 Wrocław, Poland

Abstract: Applying the condition monitoring technology to industrial processes can help detect faults in time, minimise their impact and reduce the cost of unplanned downtime. Since the introduction of the Industry 4.0 paradigm, many companies have been investing in the development of such technology for drive systems. Permanent magnet synchronous motors (PMSMs) have recently been used in many industries. Therefore, the issues of condition monitoring of PMSM drives are important. This study proposes and compares diagnostic schemes based on the stator phase currents (SPCSCs) signal for condition monitoring and fault diagnosis of PMSM stator winding faults. The continuous wavelet transform (CWT) is used for the extraction of the symptoms of interturn short circuits in PMSM stator winding. Machine learning algorithms are applied to automate the detection and classification of the faults. The concept for an original and intelligent PMSM stator winding condition monitoring system is proposed.

Keywords: *fault diagnosis • interturn short circuits • continuous wavelet transform • machine learning • permanent magnet synchronous motor*

1. Introduction

Excellent dynamics, high power density and torque inertia ratio, and a wide range of speed control make permanent magnet synchronous motors (PMSMs) one of the most attractive motor types for modern drive systems (Dai et al., 2021). PMSMs have been used in various applications, including automotive, transportation, aviation, and HVAC (Zhou et al., 2021b). Despite their reliability, PMSMs are subject to electrical (stator winding), magnetic (demagnetisation) and mechanical (eccentricity, unbalance, bearings) faults. According to statistics, stator winding faults are one of the most common sources of AC motor faults, accounting for more than 36% of all failures, depending on the size and type of the machine (He et al., 2014; O'Donnell, 1985).

Stator winging faults are highly destructive in nature (Orlowska-Kowalska et al., 2022). They usually start with a difficult-to-detect short circuit between adjacent turns and then spreads to subsequent coils and phases, leading to a critical motor failure in a short time. The motor winding can be replaced if the stator winding fault is detected at an early stage. Nevertheless, core damage caused by a phase-to-ground short circuit is irreversible. Therefore, detection before catastrophic failure can be achieved if interturn short circuit (ITSC) faults are detected by appropriate condition monitoring systems at an early stage (Wolkiewicz et al., 2016).

The extraction of electric motor fault symptoms is typically based on the processing of various types of diagnostic signals, such as stator phase current (SPCSC), mechanical vibration, temperature and stray (radial or axial) flux (Bhuiyan et al., 2020; Chen et al., 2019; Orlowska-Kowalska et al., 2022). Among them, SPCSC is most often used for stator winding fault diagnosis (Kim, 2011). The most popular methods of processing this signal to extract the fault

* Email: marcin.wolkiewicz@pwr.edu.pl

symptoms of the PMSM stator windings are frequency-domain analysis methods, such as motor current signature analysis (MCSA) which is based on the application of fast Fourier transform (FFT) (Krzysztofiak et al., 2020; Haddad and Strangas, 2016). However, although frequency-domain analysis methods have many advantages, they also have limitations, such as time information loss when moving from the time domain to the frequency domain. Time–frequency (TF) analysis methods do not have such drawbacks. In addition to extraction of the symptoms of damage, they allow for determining when the fault occurred. These methods include short-time Fourier transform (STFT) (Pietrzak and Wolkiewicz, 2022; Zanardelli et al., 2007), Hilbert–Huang transform (HHT) (Urresty et al., 2009) and continuous wavelet transform (CWT). However, in the case of the CWT, despite its many advantages and proven effectiveness in fault diagnosis of induction motors (Zaman et al., 2019), it has not been extensively studied for its use in extracting the symptoms of PMSM stator winding faults.

The signal processing algorithms can be used for the extraction of fault symptoms and the determination of certain fault indicators. Nevertheless, modern diagnostic systems should also guarantee automatic inference of the motor condition. In recent years, artificial neural networks (ANNs) have been most often used in this field. Shallow neural networks, such as the multilayer perceptron (MLP) (Skowron et al., 2022a) or radial basis function neural network (Ewert et al., 2021), are particularly popular, as well as those with a deep structure, especially convolutional neural networks (CNNs)(Pietrzak et al., 2022; Skowron et al., 2022b; Song et al., 2023). However, classical and computationally uncomplicated machine learning (ML) algorithms, such as k-nearest neighbour (KNN) model, with effective signal preprocessing algorithms to extract fault symptoms may be sufficient.

There is a lack of studies that combine advanced signal processing methods, such as CWT, with classic ML algorithms for condition monitoring of the PMSM stator winding. Thus, the present study aims to analyse the applicability of the CWT analysis of symmetrical components of SPCSCs in fault diagnosis of PMSM stator windings and then to verify the effectiveness of selected ML-based fault classifiers in the automation of the condition monitoring process of the PMSM stator winding. Classical ML algorithms were chosen, which are less mathematically and computationally complex than solutions based on deep learning, achieving short training and model response times. The main contributions of this research are as follows:

(1) Extraction of the incipient PMSM stator winding fault (ITSC) symptoms from the SPCSC signal using CWT analysis.
(2) Experimental verification and comparison of the effectiveness of ML-based PMSM stator winding condition classifiers.
(3) Improving the classification effectiveness of the fault classifiers by properly tuning their hyperparameters.
(4) Development of an original and fully automatic ML-based stator winding condition monitoring system that operates online and detects and classifies ITSCs at an incipient stage.

The article is organised as follows: Section 2 describes the theoretical basis of the methods proposed in this study. Section 3 presents the motor test stand. Section 4 presents the results of experimental verifications, including the ITSC fault symptom extraction step, as well as the training, testing and comparison of the ML-based fault classifiers. The main conclusions of this research are provided in Section 5.

2. Methods

The method of PMSM stator winding condition monitoring proposed in this article consists of two main parts: The first realises the extraction of the ITSCs symptoms and is based on TF analysis (CWT) of the SPCSCs. The extracted symptoms will then be used in the second module as elements of the input vectors of fault classifiers, which are based on ML. The classifier models tested and compared are KNN, support vector machine (SVM) and MLP.

2.1. CWT

TF analysis methods are popular in fault diagnosis because information about the time of occurrence of a given component is not lost after signal processing (Cohen, 1989). One of the most common and classic TF analysis methods is STFT. STFT can be used to observe frequency components at a specific time interval. However, the size of the window that is sliding along with the time axis in STFT analysis and therefore the time and frequency

resolution is fixed (Diao et al., 2022). The scale factor that is used in CWT analysis, the length of the time window, is adjustable. Therefore, it is possible to achieve good resolution in both TF domains, overcoming the limitations of STFT.

CWT is an effective approach for the extraction of the fault features (Shao et al., 2020). Thanks to the good TF resolution, the CWT has been used also in the fault diagnosis field. Nevertheless, its effectiveness has been verified for the diagnosis of induction motor faults (Diao et al., 2022; Shao et al., 2020; Zaman et al., 2019). The CWT of a signal $x(t)$ can be expressed by the following equation (Diao et al., 2022):

$$\mathrm{CWT}(\tau,a) = \int x(t)\psi_{a,\tau}^{*}(t)dt = \frac{1}{\sqrt{|a|}}\int x(t)\psi^{*}\left(\frac{t-\tau}{a}\right)dt, \tag{1}$$

where a is the scale factor, τ is the parameter of the translation in the time domain, ψ is the mother wavelet, $\psi^{*}(\cdot)$ is the complex conjugate of function $\psi(\cdot)$ and $\psi_{a,\tau}$ is the baby wavelet (translated and scaled version of the mother wavelet ψ (Shao et al., 2020)):

$$\psi_{a,\tau} = \frac{1}{\sqrt{|a|}}\psi\left(\frac{t-\tau}{a}\right). \tag{2}$$

2.2. Applied machine learning models

2.2.1. KNNs

The first ML model analysed is based on the KNN algorithm, which is one of the basic and most popular algorithms in the field of data classification. It assumes that the classes (labels) of the data included in the training dataset are known. For the new data, this algorithm compares the features of the new data with those of the training dataset. The distance between the new point and the points included in the dataset is calculated. The label of the new input data is the label that appears most frequently among the nearest K points (Ma and Chi, 2022). Different metrics for calculating the distance between the neighbouring points have been proposed in the literature. Introducing feature vectors: $A = (x_1, x_2,..., x_n)$ and $B = (y_1, y_2,..., y_n)$, where n denotes the dimensionality of the feature space, the most popular distance metrics (Euclidean, Minkowski, Mahalanobis, correlation) can be calculated as follows:

$$d_{\mathrm{Euclidean}}(A,B) = \sqrt{\sum_{i=1}^{n}(x_i - y_i)^2}, \tag{3}$$

$$d_{\mathrm{Minkowski}}(A,B) = \left(\sum_{i=1}^{n}|x_i - y_i|^r\right)^{\frac{1}{r}}, \tag{4}$$

$$d_{\mathrm{Mahalanobis}}(A,B) = \sqrt{\left(\frac{x_1 - y_1}{\sigma_1}\right)^2 + \left(\frac{x_2 - y_2}{\sigma_2}\right)^2}, \tag{5}$$

$$d_{\mathrm{Correlation}}(A,B) = \frac{\sum_{i=1}^{n}(x_i - \mu_i)(y_i - \mu_i)}{\sqrt{\sum_{i=1}^{n}(x_i - \mu_i)^2\sum_{i=1}^{n}(y_i - \mu_i)^2}}, \tag{6}$$

where n is the feature space dimension; σ is the standard deviation; $\overline{x}$ and $\overline{y}$ are mean values of x and y vectors, respectively; r is the order of the Minkowski distance metric.

2.2.2. Support vector machine

The SVM algorithm, proposed by Vapnik (2000), is an ML algorithm that is based on structural risk minimisation. The basic form of the SVM algorithm is a binary classifier that learns a linear hyperplane that separates data points belonging to different classes as much as possible, which maximises the margin between two classes. The support vectors are the nearest data points that define the margin (Namdari and Jazayeri-Rad, 2014).

Given a known training sample set $S = \{(x_i, y_i), i = 1,\ldots, M\}$, M is the number of samples and each sample $x_i \in R^d$. The data included in the training dataset are assumed to have two classes: positive class and negative class. These two classes are associated with a label, $y_i \in \{+1, -1\}$, for positive and negative classes, respectively. For the linearly separable data, it is possible to define the hyperplane that separates the data (Namdari and Jazayeri-Rad, 2014; Widodo and Yang, 2007):

$$f(\mathbf{x}) = \mathbf{w}^T \mathbf{x} + b = 0, \tag{7}$$

where $\mathbf{W}$ is a vector of a d-dimension and b is a scalar bias.

The vectors $\mathbf{W}$ and b are used to define the separating hyperplane position. For the case that is linearly separable, to find the optimal hyperplane—the hyperplane that provides the maximum classification margin and better generalisation availability, a positive slack variable for each training sample is defined ζ_i. To find this hyperplane, the following optimisation problem has to be solved (Widodo and Yang, 2007; Zhou et al., 2021a):

$$\min_{\mathbf{w},b}\left(\frac{\|\mathbf{w}\|^2}{2} + C\sum_{i=1}^{M} \xi_i \right), \tag{8}$$

subject to

$$\begin{cases} y_i(\mathbf{w}^T\mathbf{x}_i + b) \geq 1 - \xi_i, & i = 1,2,\ldots,M \\ \xi_i \geq 0, & i = 1,2,\ldots,M \end{cases}, \tag{9}$$

where C is the regularisation parameter determining the trade-off between the minimisation of the classification error and maximisation of the margin between two classes.

To solve the aforementioned optimisation problem, by introducing Lagrange multiplier $\alpha_i > 0$ and subject to (11), the dual quadratic optimisation problem is obtained (Widodo and Yang, 2007):

$$\max_{\alpha} \ L(\alpha) = \sum_{i=1}^{N_s} \alpha_i - \sum_{i,j=1}^{N_s} \alpha_i\alpha_j y_i y_j x_i x_j \tag{10}$$

subject to

$$\alpha_i \geq 0, \ i = 1,2,\ldots,N_s, \sum_{i=1}^{N_s} \alpha_i y_i = 0 \tag{11}$$

The kernel trick is utilised to make the linear classification possible. Kernel functions are used to transform the data from the original input space to a high-dimensional feature space (Zhou et al., 2021a). There are different kernel functions known in the literature. The most popular from them are the linear, polynomial and Gaussian kernel functions. They are defined as follows:

$$K_{\text{Linear}}(x_1, x_2) = x_1^T x_2, \tag{12}$$

$$K_{\text{Gaussian}}(x_1, x_2) = e^{-\left(\frac{\|x_1 - x_2\|^2}{2\sigma^2}\right)}, \tag{13}$$

$$K_{\text{Polynomial}}(x_1, x_2) = \left(x_1^T x_2 + 1\right)^{\gamma}, \tag{14}$$

where σ is the Gaussian function width and γ is the polynomial degree.

2.2.3. MLP

Feedforward MLP is one of the most commonly used structures of the shallow neural networks, which has been used in various applications, including fault diagnosis of electric motors (Ewert et al., 2021). The MLP approximation constructs a unique model that is composed of the following layers: input layer, hidden layer(s) and output layer

(García-Cuesta et al., 2008). The operation principle of the MLPs can be explained in three main steps (Kaminski and Orlowska-Kowalska, 2015): first, input signals are preliminary scaled with input weights w_{ij}, then input signals of each hidden neuron are summed and then processed with the activation function, and at the end, output (usually linear neuron) is used for the summation of the scaled signal. Therefore, the output of the neurons, which is a function f of the weighted inputs plus a bias, can be simply expressed (García-Cuesta et al., 2008):

$$\text{out}_i = f\left(\sum_{j=1}^{n} w_{ij} x_j + b_i\right),$$

(15)

where x_j and b_i are weights and biases of the neuron i.

There are different training methods for MLPs. Nevertheless, one of the most common and fastest MLP training algorithms is the Levenberg–Marquardt optimisation (Chiddarwar and Ramesh Babu, 2010).

3. Experimental Setup

All results presented in the following sections are the experimental test results conducted on a specially prepared test bench. The photo of the experimental setup is shown in Figure 1. The motor under study is a 2.5 kW PMSM. This motor was supplied from the voltage source inverter (VSI) by Lenze, Aerzen, Germany (Topline 8400). The rated parameters of this motor are grouped in Table 1. The construction of the PMSM stator winding was specially prepared to allow the physical modelling of a selected number of ITSCs. A group of stator winding coils was led out to the terminal board. In the scope of the experimental verification, the incipient ITSCs (1÷5 shorted turns) were analysed. Given that the number of turns in each of the phases is 250, the minimum number of turns that were shorted (N_{sh} = 1) during the tests represents 0.4% of all turns in one phase. Direct ITSCs were physically modelled
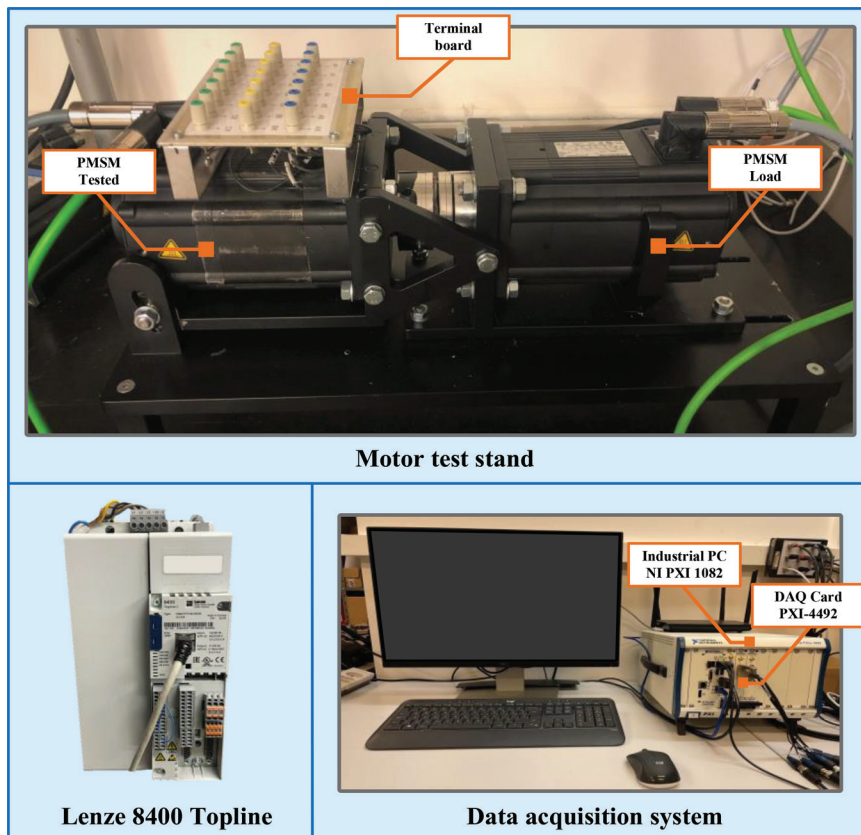

Fig. 1. Overview of the experimental setup. PMSM, permanent magnet synchronous motor.

Parameter	Symbol	Value	Unit
Rated power	P_N	2,500	W
Rated rotation speed	n_N	1,500	r/min
Rated torque	T_N	16	Nm
Rated supply frequency	f_{sN}	100	Hz
Rated stator phase voltage	U_{sN}	325	V
Rated SPCSC	I_{sN}	6.6	A
Number of rotor pole pairs	p_p	4	-
Number of stator turns (in one phase)	N_s	2×125	-

PMSM, permanent magnet synchronous motor; SPCSC, stator phase current.

Table 1. Rated parameters of the tested PMSM.

with a wire without the additional resistor to limit the current in the shorted-circuit with an additional resistor. To verify the impact of the ITSC under different operating conditions, a second PMSM with a nominal power of 4.7 kW was coupled to the PMSM under test. The SPCSCs were measured using LEM LA 25-NP current transducers. The DAQ NI PXI-4492 measurement card housed inside an industrial PC by National Instruments, Austin, TX, US (PXI 1082) was used for the diagnostic signal acquisition purposes.

4. Results and Discussion

4.1. Influence of ITSCs on the stator current symmetrical component waveforms of PMSM drive

The SPCSC signal contains information about various types of motor faults, and it is non-invasive and easy to measure. This makes it one of the most popular signals in AC motor fault diagnosis. The ITSC in the PMSM stator winding causes an asymmetry of the SPCSCs. This asymmetry affects the values of the SPCSC. The instantaneous values of the SPCSC are determined using the 90° time-domain shift operator (S_{90}) and are calculated as follows (Iravani and Karimi-Ghartemani, 2003):

$$\begin{bmatrix} i_1 \\ i_2 \end{bmatrix} = \frac{1}{3} \begin{bmatrix} i_{sA} - \frac{1}{2}(i_{sB} + i_{sC}) + \frac{\sqrt{3}}{2} S_{90}(i_{sB} - i_{sC}) \\ i_{sA} - \frac{1}{2}(i_{sB} + i_{sC}) - \frac{\sqrt{3}}{2} S_{90}(i_{sB} - i_{sC}) \end{bmatrix} \tag{16}$$

where i_1 and i_2 are the instantaneous values of the positive and negative SPCSC sequence components and i_{sA}, i_{sB} and i_{sC} are the instantaneous values of the stator current in phases A, B and C.

The waveform of i_1 for various conditions of the stator winding—momentary short-circuiting successively 1–5 turns (N_{sh}) for various T_L levels in the range from 0 to the rated value T_N with a step of $0.2T_N$—is shown in Figure 2. The analysis of the waveform shows that the changes in the amplitude of the i_1 caused by the ITSCs are noticeable, but the influence of the T_L level is significantly higher. The percentage increase in the amplitude of i_1 by ITSC, especially at the early stage of the fault, decreases as the motor load increases. The effects of ITSC in the PMSM stator winding can also be seen in the i_2 waveform. The waveform of this component for the same conditions as presented for i_1 is shown in Figure 3. Compared to the i_1 component, it is noticeable that the impact of the load torque level is much smaller. In addition, a significant increase due to ITSC is visible. This is extremely important because in the fault diagnosis, there is a need to look for fault indicators whose values are no drive system operating conditions dependent and only changes as a result of the fault. In the case of both i_1 and i_2 waveforms, as T_L, increases, the increase in amplitude due to the fault decreases for the initial stage of the fault. It is especially visible for $T_L = \{0.6\ T_N, 0.8\ T_N, T_N\}$. Therefore, only based on the waveforms of these components, effective fault diagnosis and condition monitoring of PMSM stator winding would be hampered. In this regard, in the scope of this research, CWT analysis is used to extract the symptoms that are more sensitive to the ITSCs, also at the initial stage of the fault.
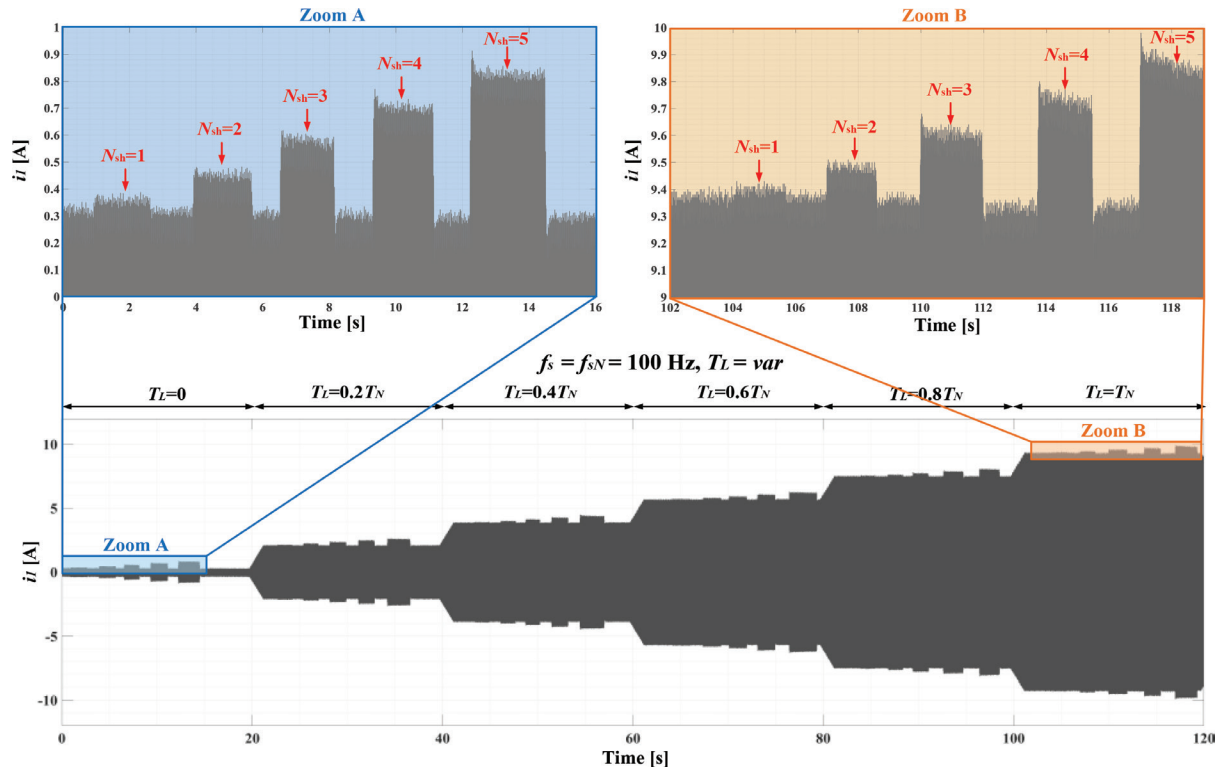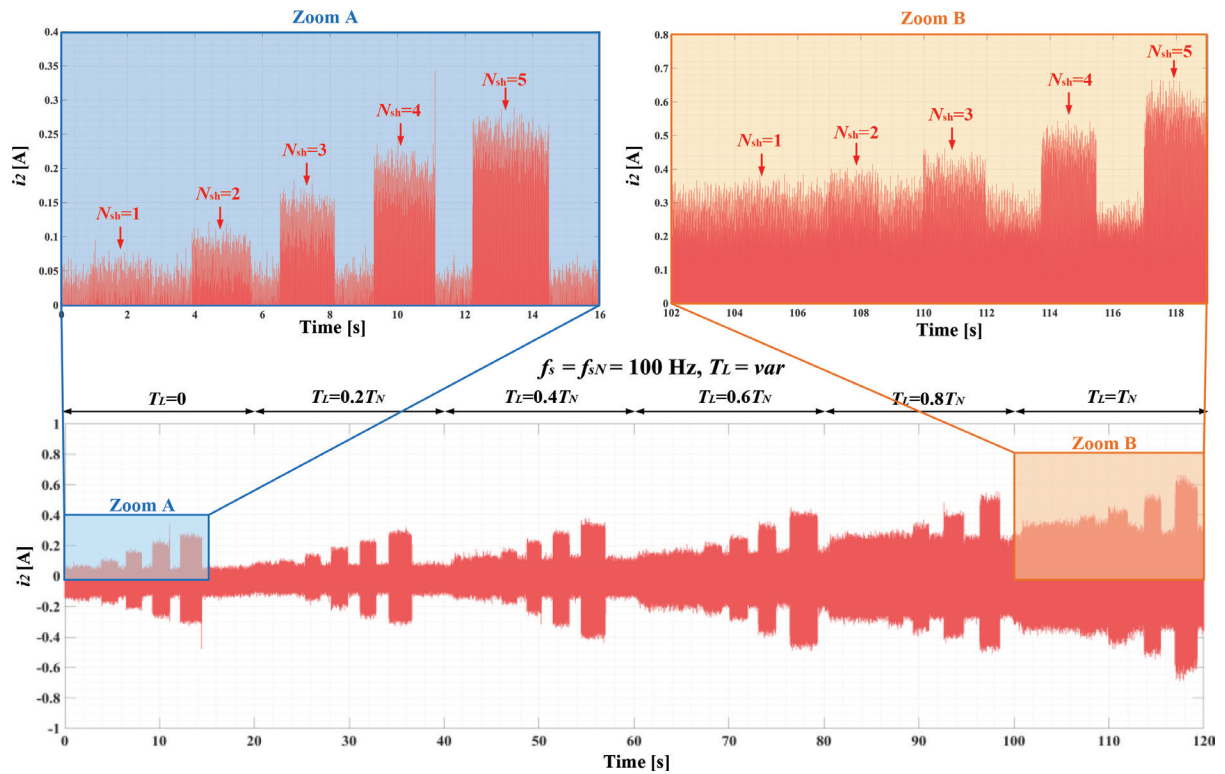
Fig. 2. Waveform of i_1 for different stator winding conditions (N_{sh}) and motor operating conditions, experimental verification for T_L = var and $f_s = f_{sN}$ = 100 Hz.

Fig. 3. Waveform of the i_2 for different stator winding conditions (N_{sh}) and motor operating conditions, experimental verification for T_L = var and $f_s = f_{sN}$ = 100 Hz.

4.2. CWT-based PMSM stator winding fault symptom extraction

CWT scalograms of the i_1 signal for the undamaged stator winding and with ITSC of three turns in phase A for different T_L levels are shown in Figure 4. The scalograms show a notable increase in the amplitude value of the frequency component connected with the fundamental harmonic ($f_s = f_{sN} = 100$ Hz) as the T_L level increases. The analysis of these scalograms did not reveal frequency components whose amplitude value increased significantly as a result of damage. Nevertheless, the f_s component amplitude carries information about the T_L level. The i_2 signal CWT scalograms for the same stator and PMSM operating conditions are presented in Figure 5. Comparing these scalograms, a notable increase in the amplitude value of the f_s caused by the occurrence of the ITSC is visible. Moreover, no significant effect of T_L on the value of this amplitude can be seen. Nevertheless, further analysis is needed, especially for various N_{sh}, to finally assess its usefulness.

To verify the increase in the coefficient values related to the f_s component in the CWT scalogram of i_1 and i_2 signals for different severity values of the stator fault, the experimental verification for momentary ITSCs (for 1÷2s) and different T_L levels is conducted. In Figure 6, the i_1 CWT scalogram (Figure 6a) and amplitude changes of the CWT coefficient of the f_s component $|CWT_{i1}(f_s,t)|$ (Figure 6b) during the cyclic short-circuiting of 1–5 turns at each of the analysed T_L levels are shown. The value of $|CWT_{i1}(f_s,t)|$ increases significantly as a result of the T_L increase, as previously proven, and only slight changes resulting from ITSC are present.

Figure 7 shows the i_2 CWT scalogram and $|CWT_{i2}(f_s,t)|$ value for the same PMSM operating and stator winding conditions as for the i_1 analysis. The value of the $|CWT_{i2}(f_s,t)|$ increases significantly after the occurrence of the ITSC over the entire range studied. This increase is also notable at the incipient stage of the fault ($N_{sh} = 1$). In addition, the waveforms of the $|CWT_{i2}(f_s,t)|$ values for different f_s were analysed, as shown in Figure 8. The increase is visible for the corresponding coefficient at a given frequency for the entire range analysed. Based on these considerations, it can be concluded that this may be a good indication of PMSM stator winding faults.

The presented results of the experimental verification are obtained for the Morse wavelet. Nevertheless, the analysis was done for different types of wavelets: Morse, Morlet (Gabor) and bump wavelets. The theoretical details and properties of these wavelets are described in detail in previous studies (Gao et al., 2009;
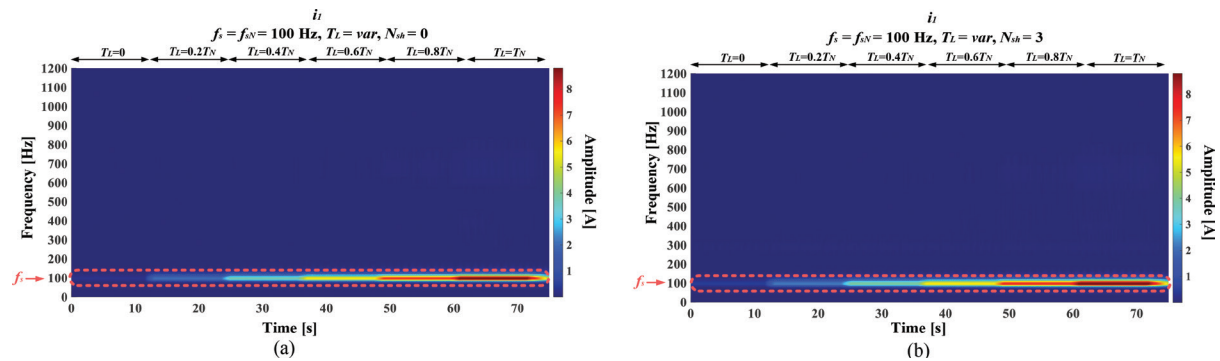

Fig. 4. CWT scalograms of i_1: (a) undamaged stator winding ($N_{sh} = 0$), (b) damaged stator winding ($N_{sh} = 3$) for T_L = var and $f_s = f_{sN} = 100$ Hz. CWT, continuous wavelet transform.
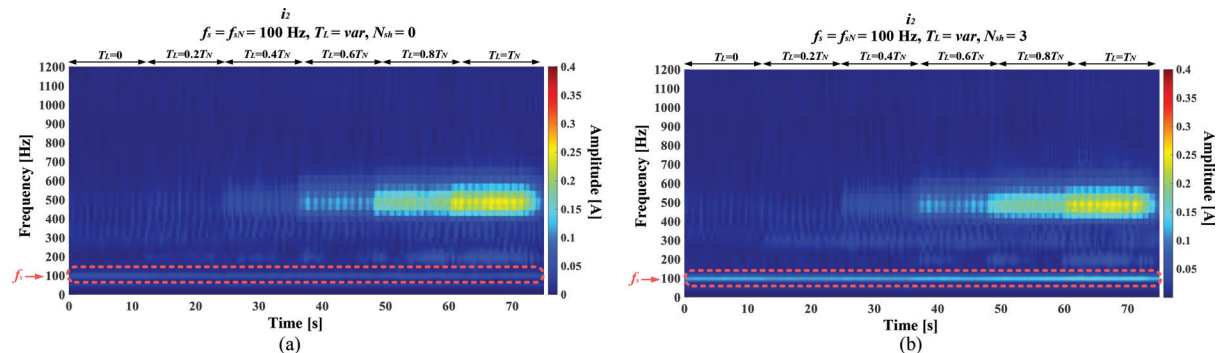

Fig. 5. CWT scalograms of i_2: (a) undamaged stator winding ($N_{sh} = 0$), (b) damaged stator winding ($N_{sh} = 3$) for T_L = var and $f_s = f_{sN} = 100$ Hz. CWT, continuous wavelet transform.
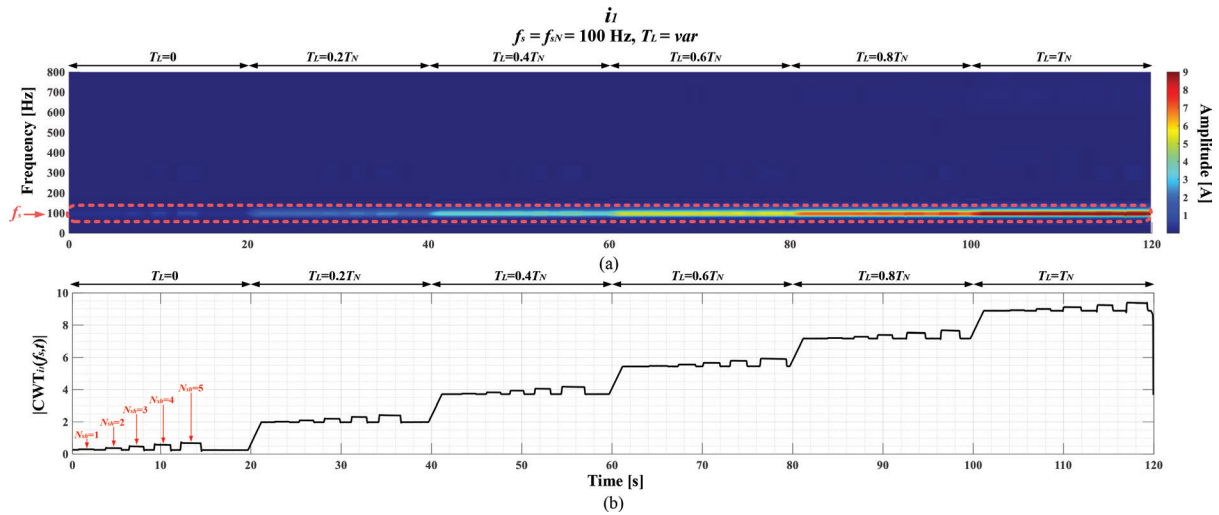
Fig. 6. (a) i_1 CWT scalogram and (b) value changes of the $|\text{CWT}i_1(f_s,t)|$ for the short-circuiting of 1–5 turns and T_L = var, f_s = f_{sN} = 100 Hz. CWT, continuous wavelet transform.
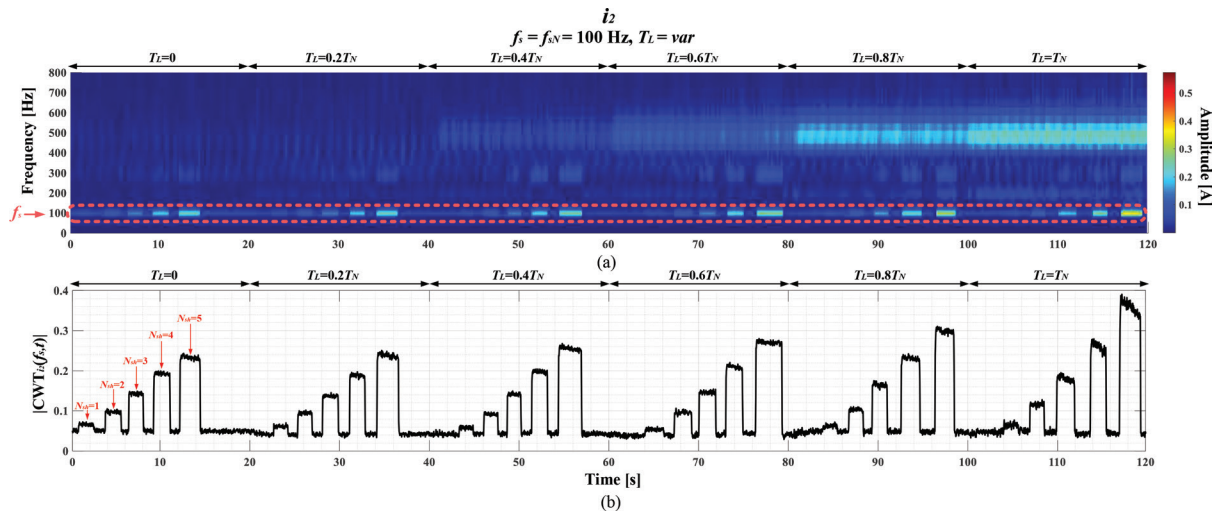

Fig. 7. (a) i_2 CWT scalogram and (b) value changes of the $|\text{CWT}i_2(f_s,t)|$ for the short-circuiting of 1 to 5 turns and T_L = var, f_s = f_{sN} = 100 Hz. CWT, continuous wavelet transform.

Lilly and Olhede, 2009, 2012). Figure 9 shows the comparison of $|\text{CWT}_{i2}(f_s,t)|$ for the same conditions as presented in Figure 7, but for different types of wavelet. The greatest sensitivity of the $|\text{CWT}_{i2}(f_s,t)|$ value to the ITSC is obtained for the Morse wavelet. Therefore, this type of wavelet will be used in the next part of the research.

The experiments were carried out for various T_L levels and power supply voltage frequencies f_s (rotation speeds). The effect of the stator winding fault severity (N_{sh}) and T_L level on the increase in the $|\text{CWT}_{i2}(f_s,t)|$ value is shown in Figure 10a. The effect of the f_s value is shown in Figure 10b. These charts show the increase in the $|\text{CWT}_{i2}(f_s,t)|$ value caused by the ITSC is significant over the entire range of T_L and f_s analysed. Nevertheless, as the value of f_s decreases, the damage sensitivity is slightly lower.

4.3. ML-based automation of the PMSM stator winding fault classification

The fault classifier models are trained based on the information obtained in the previous stage of the research, namely the extraction of symptoms of this type of damage. It is proven that in the CWT scalogram of the i_1 coefficients associated with the f_s component, $|\text{CWT}_{i1}(f_s,t)|$ contains information about the T_L level, while the frequency component f_s in the i_2 CWT scalogram is a very good indicator of ITSCs. Therefore, these values are included in the input vector of the models under study. The third and last component of the input vector is the f_s value.
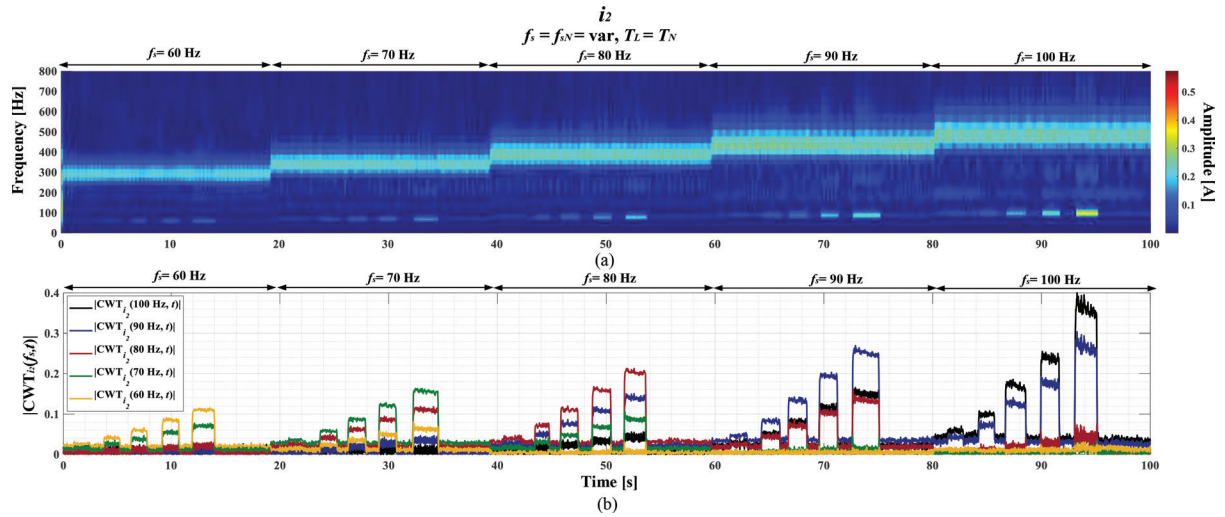
Fig. 8. (a) i_2 CWT scalogram and (b) value changes of the $|\text{CWT}i_2(f_s,t)|$ for the short-circuiting of 1 to 5 turns ($T_L = T_N$, f_s = var). CWT, continuous wavelet transform.
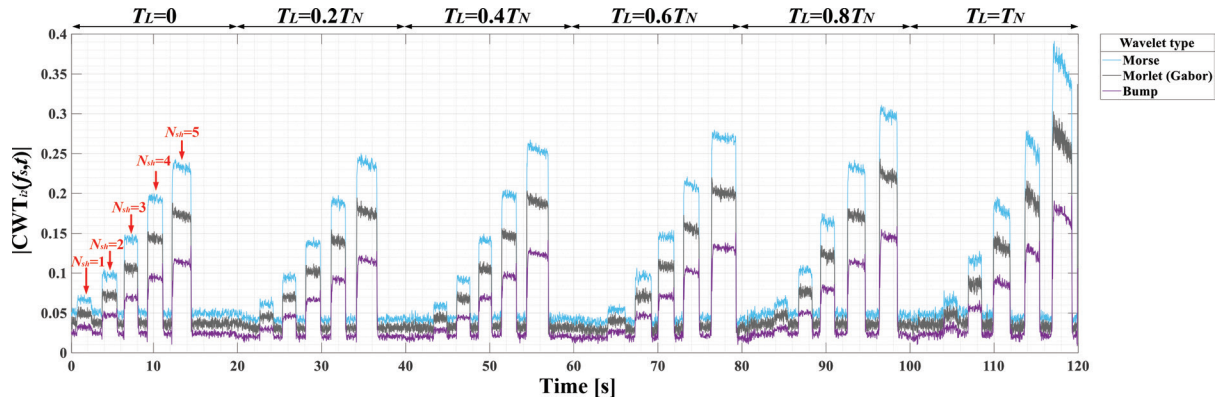

Fig. 9. Value changes of $|\text{CWT}i_2(f_s,t)|$ for the short-circuiting of 1 to 5 turns and different types of wavelet (T_L = var, $f_s = f_{sN}$ = 100 Hz). CWT, continuous wavelet transform.

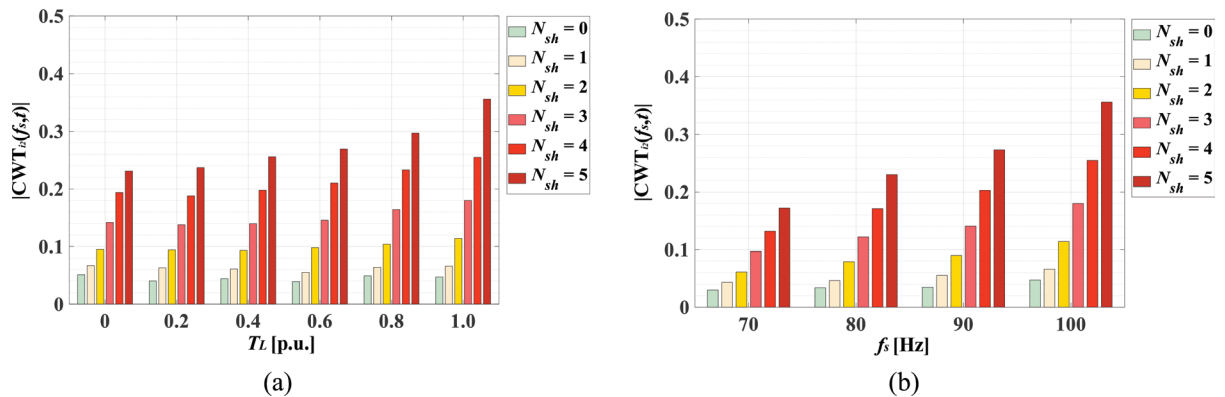**Fig. 10.** Effect of N_{sh} and (a) T_L ($f_s = f_{sN}$ = 100 Hz). (b) f_s ($T_L = T_N$) on the value of the $|\text{CWT}i_2(f_s,t)|$ coefficient. CWT, continuous wavelet transform.

4.3.1. Training and off-line verification of the ML-based models

The dataset collected through experimental research consists of 5,400 vectors of the following form: $\boldsymbol{X} = [|\text{CWT}_{i1}(f_s,t)|,$ $|\text{CWT}_{i2}(f_s,t)|, f_s]$. For each of the load torques T_L = {0; $0.2T_N$; $0.4T_N$; $0.6T_N$; $0.8T_N$; T_N}, number of shorted turns N_{sh} = {0; 1; 2; 3; 4; 5} and power supply frequencies f_s = {80 Hz; 90 Hz;100 Hz}), there are 50 vectors included in

the dataset (50 × 6 × 6 × 3 = 5,400). The dataset was randomly divided into 70% for the training and 30% for the offline tests.

4.3.1.1. KNN model

The key parameters of the KNN algorithm include the number of nearest neighbours and distance metric. To select the model parameters that will provide the best accuracy, different hyperparameter values are analysed. The accuracy of the model is the number of correctly classified states of the stator winding $n_{correct}$ to the number of vectors included in the training dataset N:

$$\text{Accuracy} = \frac{n_{correct}}{N} \cdot 100\% . \tag{17}$$

The accuracies of the KNN ITSC classifier model for different hyperparameters are grouped in Table 2. According to the results, the lowest accuracy is achieved by the KNN model with the correlation distance. The highest accuracy of 99.9% is achieved by KNN models for $K = 5$ and the Euclidean, Minkowski and Mahalanobis distance. Training times of these models are 0.691 s, 0.781 s and 1.790 s, respectively. Therefore, taking into account these times, the KNN model with the Euclidean distance metric is chosen for further analysis.

The achieved classification effectiveness C_{EFF} (the ratio of the correctly classified stator winding conditions to the sum of the testing vectors) is as high as 99.75%. The confusion matrix for the model responses to the test vectors is presented in Figure 11a. Few misclassifications are visible only in the case of one shorted turns in the stator winding.

K [-]	Symbol			
	Euclidean (%)	Minkowski (%)	Mahalanobis (%)	Correlation (%)
1	99.6	99.6	99.7	84.3
2	99.7	99.7	99.7	84.5
3	99.7	99.7	99.8	85.5
4	99.7	99.7	99.8	85.7
5	99.9	99.9	99.9	86.2
10	99.8	99.8	99.8	86.0
25	99.8	99.8	99.8	85.8
50	99.8	99.8	99.8	84.8
100	78.5	75.7	79.6	60.0

KNN, k-nearest neighbour.

Table 2. Results (accuracy) of the KNN model for different values of hyperparameters.
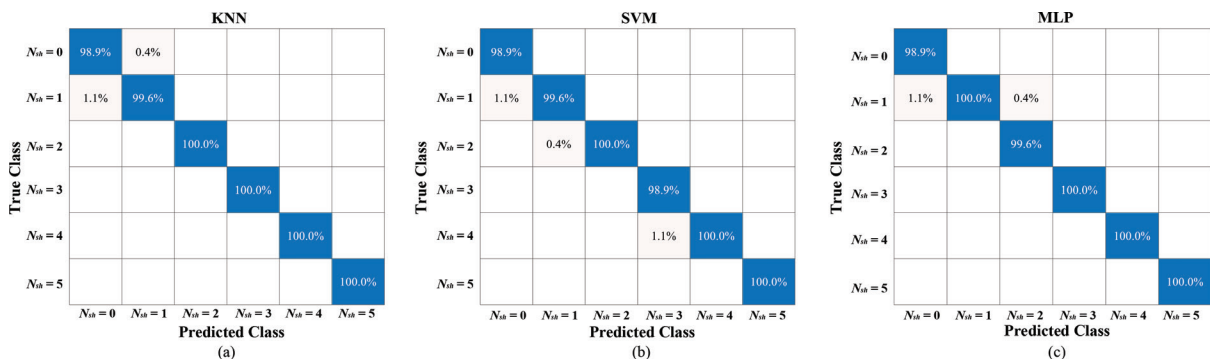

Fig. 11. Confusion matrix for the responses to the test vectors of (a) KNN, (b) SVM and (c) MLP models. KNN, k-nearest neighbour; MLP, multilayer perceptron.

4.3.1.2. SVM

The preparation of an SVM-based fault classifier model involves the selection of a kernel function that will ensure the highest accuracy of the model. The model accuracies of the SVM classifier for different kernel functions are grouped in Table 3.

The results show that the SVM model with the linear kernel function is characterised by the lowest model accuracy equal to 97.8%. The SVM model with cubic kernel achieved the highest accuracy of 99.8%, as well as with the Gaussian kernel function with widths of 0.4 and 0.5. For further tests, the SVM with Gaussian kernel function with $\sigma = 0.4$ is selected due to its shortest training time (1.821 s) compared to the other SVMs, which also achieved an accuracy of 99.8%. After analysing the model accuracy for different kernel functions, the results of the selected models for the test vectors are verified. The confusion matrix for these responses is shown in Figure 11b. As can be seen, there are only isolated cases of misclassification. The classification effectiveness achieved is equal to 99.57%. Compared to KNN, there are misclassifications not only between the undamaged winding and one shorted turn but also between 3 and 4 shorted turns.

4.3.1.3. MLP

In the case of the MLPs, the most important is the selection of an appropriate structure of the network: the number of hidden layers and neurons in each layer. One of the most common methods to select the most suitable neural network structure for the selected application is the constructivist approach. In the scope of this research, the Levenberg–Marquardt gradient algorithm is used. The maximum number of epochs is set to 1,000. The accuracy of the MLP model for different neural network structures is grouped in Table 4. The MLP with the least complex network structure—only one hidden layer with five neurons—achieved the lowest accuracy (99.1%). An accuracy of 99.9% was achieved by MLPs with two structures: one hidden layer with 15 neurons and two hidden layers with 7 and 11 neurons. To choose a less complex structure, the MLP model with one hidden layer {3-15-1} is adopted for further tests. The C_{EFF} achieved by this model is equal to 99.75%. The confusion matrix for the responses for the test vectors is presented in Figure 11c.

Kernel function	σ [-]	Accuracy (%)
Linear	-	97.8
Quadratic		98.9
Cubic		99.8
	0.1	99.6
	0.2	99.6
Gaussian	0.3	99.7
	0.4	99.8
	0.5	99.8

Table 3. Results (accuracy) of the SVM model for different values of hyperparameters.

Neural network structure	Accuracy (%)
{3-5-1}	99.1
{3-7-1}	99.4
{3-9-1}	99.7
{3-13-1}	99.7
{3-15-1}	99.9
{3-5-9-1}	99.7
{3-7-11-1}	99.9

MLP, multilayer perceptron.

Table 4. Results (accuracy) of the MLP model for different network structures.

4.3.2. General workflow and verification of the proposed PMSM stator winding condition monitoring system during online operation

The combination of the proposed ITSC symptom extraction method (CWT) and the developed ML-based models (KNN, SVM, MLP) make it possible to prepare an automatic condition monitoring system for PMSM stator windings. The structure of the developed system is presented in Figure 12. The following key elements of this methodology can be distinguished: (1) the SPCSCs signal measurement and calculation of its symmetrical components, (2) CWT analysis of the SPCSCs and (3) automatic ML-based stator winding condition classification. A more detailed flow diagram depicting the concept proposed in this work is shown in Figure 13.
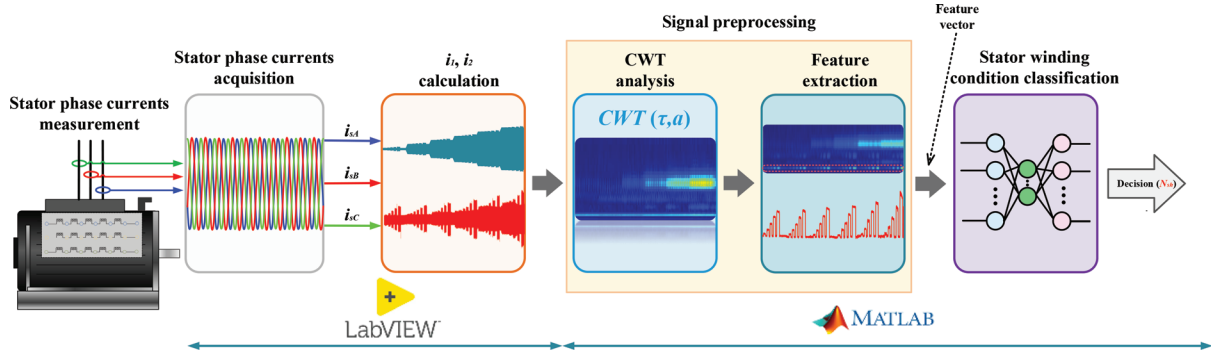

Fig. 12. General workflow of the proposed condition monitoring system. CWT, continuous wavelet transform.
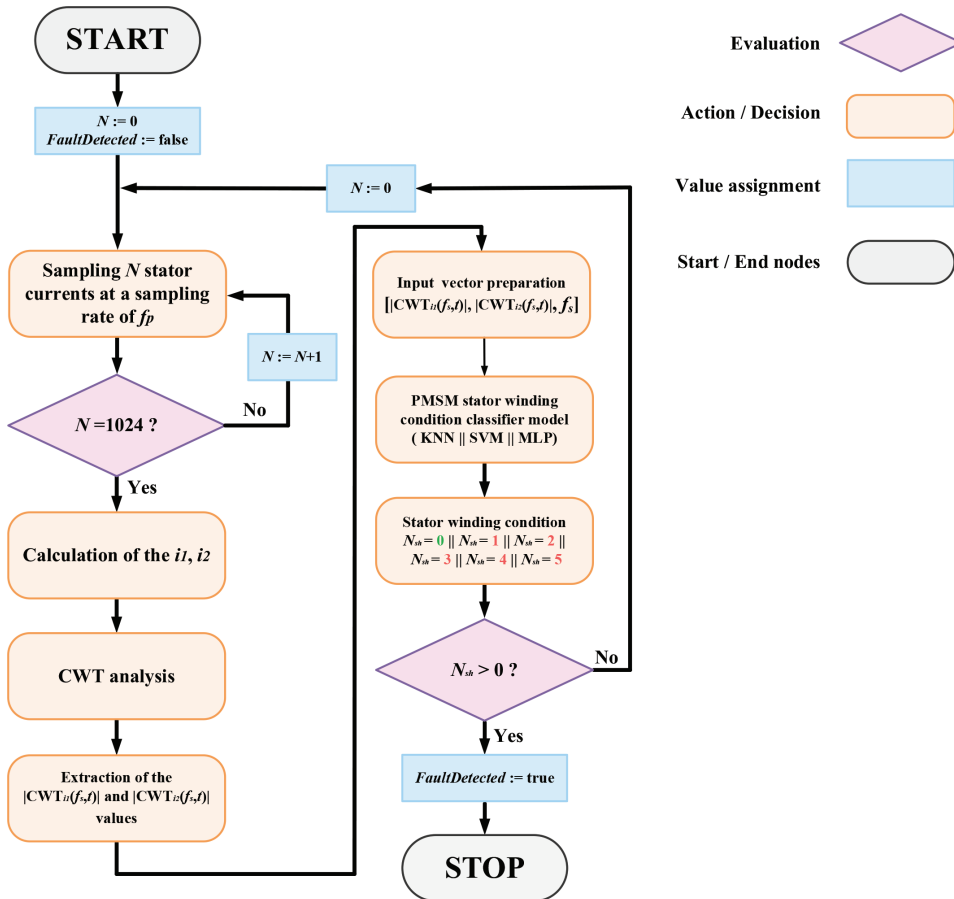

Fig. 13. Detailed flow diagram representing the proposed PMSM stator winding condition classification schemes proposed in this work. CWT, continuous wavelet transform; PMSM, permanent magnet synchronous motor.
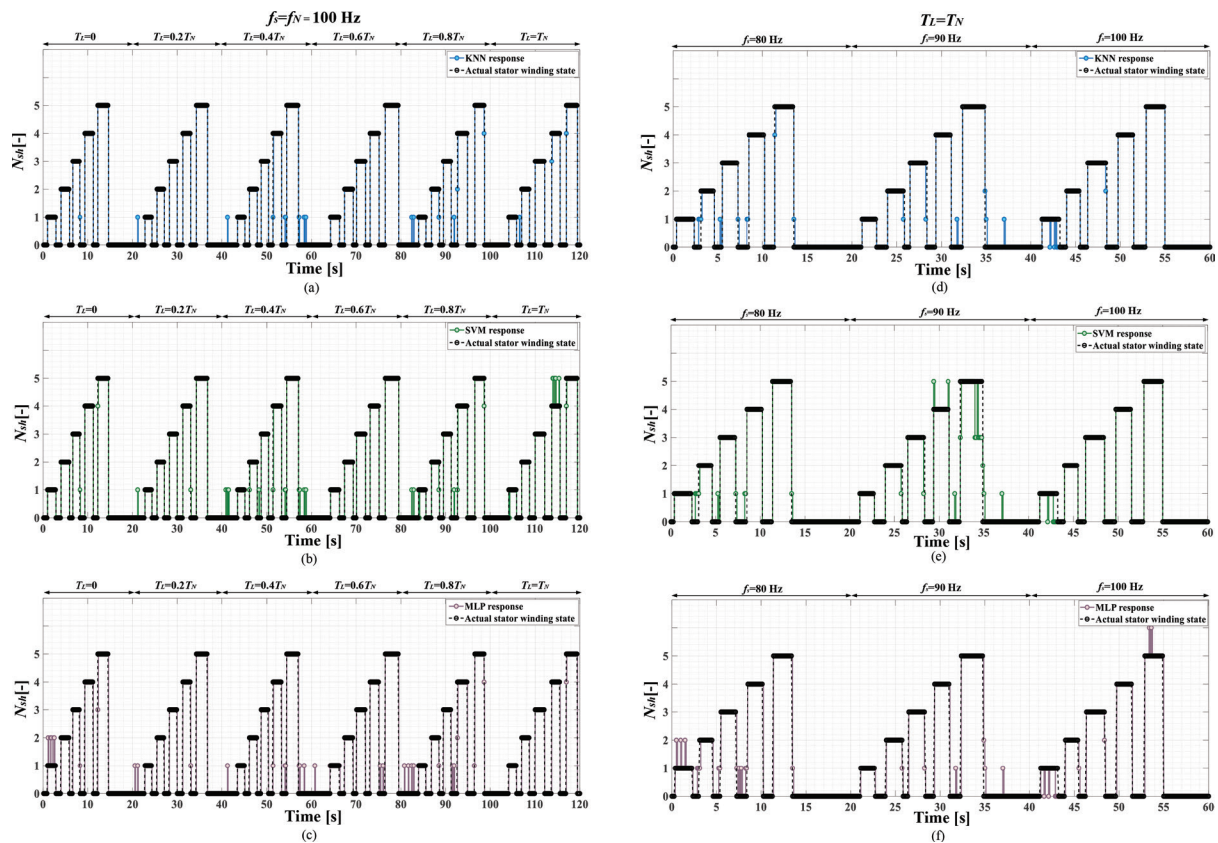
Fig. 14. Real conditions of the PMSM stator winding and fault classifier responses during the online operation of the drive system, (a), (d) KNN, (b), (e) SVM, (c), (f) MLP. KNN, k-nearest neighbour; MLP, multilayer perceptron; PMSM, permanent magnet synchronous motor.

The proposed condition monitoring system was tested during the online operation of the PMSM drive. During this test, 1–5 turns were sequentially sorted for 1–2s, gradually increasing (1) the T_L level and (2) the f_s value. The actual conditions of the PMSM stator winding and the outputs of the KNN model developed are presented in Figures 14a,d for tests (1) and (2), respectively. The C_{EFF} for these tests is equal to 98.13% and 95.63%. The SVM model responses for these test scenarios are presented in Figures 14b,e. The result shows that the C_{EFF} = 96.88% for test (1) and 93.97% for test (2). The results of the verification of the MLP model are presented in Figures 14c,f. This model achieved C_{EFF} = 96.46% and C_{EFF} = 93.97%.

In the case of ITSC fault, due to its destructive nature, it is necessary to detect it in the shortest possible time. For this reason, the times of the responses of the developed classifies are also analysed. Based on the analysis of the comparison for 10,000 trials, it is proven that the response time of the KNN model is considerably shorter than that of the other analysed models. The average response time is equal to 1.8 ms for KNN, 6.0 ms for SVM and 6.3 ms for the MLP model. It is a notable advantage of the simple KNN algorithm.

5. Conclusions

This study provides a solution to the problem of automatic diagnosis of the PMSM stator winding fault at its incipient state. The CWT analysis of the SPCSC symmetrical components and ML models are proposed to solve this problem.

The experimental results confirmed the high effectiveness of the application of the CWT analysis of the SPCSC in the extraction of the symptoms of ITSCs in the PMSM stator winding at a very early stage of the fault. After tuning the parameters of the ML-based models analysed, the proposed classifiers achieved very high accuracies and classification effectiveness under various test scenarios. The tested models are also robust against operating condition changes of the PMSM drive system, thanks to the proper selection of elements (features) of the input vector. It should be marked that the highest classification effectiveness is achieved for the KNN-based fault classifier

model, which is very simple to implement and has the potential for industrial deployment. Also importantly, the average response time of this classifier is significantly shorter than that of SVM and MLP models.

The limitation of the developed system is that it can detect only the fault that was included in the training set—stator windings fault, but it can be adapted to detect other types of damages, by training the models with different datasets. Moreover, there are several research lines where the proposed research can be continued. The first one is the preparation of the embedded low-cost condition monitoring system that utilises the proposed algorithm. The second line is to develop and add to the system a module that will be responsible for locating the faulty phase.

References

Bhuiyan, E.A., Akhand, M.A., Das, S.L., Ali, F., Tasneem, Z., Island, R., Saha, D.K., Badal, F.R., Ahamed, H. Moyeen, S.I. (2020). A Survey on Fault Diagnosis and Fault Tolerant Methodologies for Permanent Magnet Synchronous Machines. *International Journal of Automation and Computing*, 17(6), pp. 763–787. doi: 10.1007/s11633-020-1250-3.

Chen, Y., Liang, S., Li, W., Liang, H. and Wang, C. (2019). Faults and Diagnosis Methods of Permanent Magnet Synchronous Motors: A Review. *Applied Sciences*, 9(10), p. 2116. doi: 10.3390/app9102116.

Chiddarwar, S. S. and Ramesh Babu, N. (2010). Comparison of RBF and MLP Neural Networks to Solve Inverse Kinematic Problem for 6R Serial Robot by a Fusion Approach. *Engineering Applications of Artificial Intelligence*, 23(7), pp. 1083–1092. doi: 10.1016/j.engappai.2010.01.028.

Cohen, L. (1989). Time-Frequency Distributions – A Review. *Proceedings of the IEEE*, 77(7), pp. 941–981. doi: 10.1109/5.30749.

Dai, Y., Ni, S., Xu, D., Zhang, L. and Yan, X.-G. (2021). Disturbance-Observer based Prescribed-Performance Fuzzy Sliding Mode Control for PMSM in Electric Vehicles. *Engineering Applications of Artificial Intelligence*, 104, p. 104361. doi: 10.1016/j.engappai.2021.104361.

Diao, N., Wang, Z., Ma, H. and Yang, W. (2022). Fault Diagnosis of Rolling Bearing under Variable Working Conditions Based on CWT and T-ResNet. *Journal of Vibration Engineering & Technologies*, 11, pp. 3747–3757. doi: 10.1007/s42417-022-00780-w.

Ewert, P., Orlowska-Kowalska, T. and Jankowska, K. (2021). Effectiveness Analysis of PMSM Motor Rolling Bearing Fault Detectors Based on Vibration Analysis and Shallow Neural Networks. *Energies*, 14(3), p. 712. doi: 10.3390/en14030712.

Gao, Y., Li, M., Huang Z. and Lu, J. (2009). A symbol rate estimation algorithm based on Morlet wavelet transform and autocorrelation. In: *2009 IEEE Youth Conference on Information, Computing and Telecommunication. IEEE*, pp. 239–242. doi: 10.1109/YCICT.2009.5382378.

García-Cuesta, E., Galván, I. M. and de Castro, A. J. (2008). Multilayer Perceptron as Inverse Model in a Ground-Based Remote Sensing Temperature Retrieval Problem. *Engineering Applications of Artificial Intelligence*, 21(1), pp. 26–34. doi: 10.1016/j.engappai.2007.03.005.

Haddad, R. Z. and Strangas, E. G. (2016). On the Accuracy of Fault Detection and Separation in Permanent Magnet Synchronous Machines Using MCSA/MVSA and LDA. *IEEE Transactions on Energy Conversion*, 31(3), pp. 924–934. doi: 10.1109/TEC.2016.2558183.

He, J., Somogyi, C., Strandt, A. and Demerdash, N.A.O. (2014). Diagnosis of stator winding short-circuit faults in an interior permanent magnet synchronous machine. In: *2014 IEEE Energy Conversion Congress and Exposition (ECCE). IEEE*, pp. 3125–3130. doi: 10.1109/ECCE.2014.6953825.

Iravani, M. R. and Karimi-Ghartemani, M. (2003). Online Estimation of Steady State and Instantaneous Symmetrical Components. *IEEE Proceedings – Generation, Transmission and Distribution*, 150(5), p. 616. doi: 10.1049/ip-gtd:20030779.

Kaminski, M. and Orlowska-Kowalska, T. (2015). Adaptive Neural Speed Controllers Applied for A Drive System with An Elastic Mechanical Coupling – A Comparative Study. *Engineering Applications of Artificial Intelligence*, 45, pp. 152–167. doi: 10.1016/j.engappai.2015.06.011.

Kim, K.-H. (2011). Simple Online Fault Detecting Scheme for Short-Circuited Turn in a PMSM through Current Harmonic Monitoring. *IEEE Transactions on Industrial Electronics*, 58(6), pp. 2565–2568. doi: 10.1109/TIE.2010.2060463.

Krzysztofiak, M., Skowron, M. and Orlowska-Kowalska, T. (2020). Analysis of the Impact of Stator Inter-Turn Short Circuits on PMSM Drive with Scalar and Vector Control. *Energies*, 14(1), p. 153. doi: 10.3390/en14010153.

Lilly, J. M. and Olhede, S. C. (2009). Higher-Order Properties of Analytic Wavelets. *IEEE Transactions on Signal Processing*, 57(1), pp. 146–160. doi: 10.1109/TSP.2008.2007607.

Lilly, J. M. and Olhede, S. C. (2012). Generalized Morse Wavelets as a Superfamily of Analytic Wavelets. *IEEE Transactions on Signal Processing*, 60(11), pp. 6036–6041. doi: 10.1109/TSP.2012.2210890.

Ma, C. and Chi, Y. (2022). KNN Normalized Optimization and Platform Tuning Based on Hadoop. *IEEE Access*, 10, pp. 81406–81433. doi: 10.1109/ACCESS.2022.3195872.

Namdari, M. and Jazayeri-Rad, H. (2014). Incipient Fault Diagnosis Using Support Vector Machines based on Monitoring Continuous Decision Functions. *Engineering Applications of Artificial Intelligence*, 28, pp. 22–35. doi: 10.1016/j.engappai.2013.11.013.

O'Donnell, P. (1985). Report of Large Motor Reliability Survey of Industrial and Commercial Installations, Part I. *IEEE Transactions on Industry Applications*, 21(4), pp. 853–864. doi: 10.1109/TIA.1985.349532.

Orlowska-Kowalska, T., Wolkiewicz, M., Pietrzak, P., Skowron, M. and Ewe, P. (2022). Fault Diagnosis and Fault-Tolerant Control of PMSM Drives– State of the Art and Future Challenges. *IEEE Access*, 10, pp. 59979–60024. doi: 10.1109/ACCESS.2022.3180153.

Pietrzak, P., Wolkiewicz, M. and Orlowska-Kowalska, T. (2022). PMSM Stator Winding Fault Detection and Classification Based on Bispectrum Analysis and Convolutional Neural Network. *IEEE Transactions on Industrial Electronics*, 70, pp. 1–11. doi: 10.1109/TIE.2022.3189076.

Pietrzak, P. and Wolkiewicz, M. (2022). Stator phase current STFT analysis for the PMSM stator winding fault diagnosis. In: *2022 International Symposium on Power Electronics, Electrical Drives, Automation and Motion* (*SPEEDAM*). *IEEE*, pp. 808–813. doi: 10.1109/SPEEDAM53979.2022.9841990

Shao, S., Yan, R., Lu, Y., Wang, P. and Gao, R. X. (2020). DCNN-Based Multi-Signal Induction Motor Fault Diagnosis. *IEEE Transactions on Instrumentation and Measurement*, 69(6), pp. 2658–2669. doi: 10.1109/TIM.2019.2925247.

Skowron, M., Krzysztofiak, M. and Orlowska-Kowalska, T. (2022a). Effectiveness of Neural Fault Detectors of Permanent Magnet Synchronous Motor Trained With Symptoms From Field-Circuit Modeling. *IEEE Access*, 10, pp. 104598–104611. doi: 10.1109/ACCESS.2022.3211087.

Skowron, M., Orlowska-Kowalska, T. and Kowalski, C. T. (2022b). Detection of Permanent Magnet Damage of PMSM Drive Based on Direct Analysis of the Stator Phase Currents Using Convolutional Neural Network. *IEEE Transactions on Industrial Electronics*, 69(12), pp. 13665–13675. doi: 10.1109/TIE.2022.3146557.

Song, Q., Wang, M., Lai, W. and Zhao, S. (2023). On Bayesian Optimization-Based Residual CNN for Estimation of Inter-Turn Short Circuit Fault in PMSM. *IEEE Transactions on Power Electronics*, 38(2), pp. 2456–2468. doi: 10.1109/TPEL.2022.3207181.

Urresty, J., Riba, J., Romeral, L., Rosero, J. and Serna, J. (2009). Stator short circuits detection in PMSM by means of Hilbert-Huang transform and energy calculation. In: *2009 IEEE International Symposium on Diagnostics for Electric Machines, Power Electronics and Drives. IEEE*, pp. 1–7. doi: 10.1109/DEMPED.2009.5292789

Vapnik, V. N. (2000). *The Nature of Statistical Learning Theory*. New York, NY: Springer New York.

Widodo, A. and Yang, B.-S. (2007). Support Vector Machine in Machine Condition Monitoring and Fault Diagnosis. *Mechanical Systems and Signal Processing*, 21(6), pp. 2560–2574. doi: 10.1016/j.ymssp.2006.12.007.

Wolkiewicz, M., Tarchala, G., Orlowska-Kowalska, T. and Kowalski, C. T. (2016). Online Stator Interturn Short Circuits Monitoring in the DFOC Induction-Motor Drive. *IEEE Transactions on Industrial Electronics*, 63(4), pp. 2517–2528. doi: 10.1109/TIE.2016.2520902.

Zaman, S. M. K., Marma, H. U. M. and Liang, X. (2019). Broken rotor bar fault diagnosis for induction motors using power spectral density and complex continuous wavelet transform methods. In: *2019 IEEE Canadian Conference of Electrical and Computer Engineering* (*CCECE*). *IEEE*, pp. 1–4. doi:10.1109/CCECE.2019.8861517.

Zanardelli, W. G., Strangas, E. G. and Aviyente, S. (2007). Identification of Intermittent Electrical and Mechanical Faults in Permanent-Magnet AC Drives Based on Time–Frequency Analysis. *IEEE Transactions on Industry Applications*, 43(4), pp. 971–980. doi: 10.1109/TIA.2007.900446.

Zhou, J., Qiu, Y., Zhu, S., Armaghani, D. J., Li, C., Nguyen, H. and Yagiz, S. (2021a). Optimization of Support Vector Machine through the Use of Metaheuristic Algorithms in Forecasting TBM Advance Rate. *Engineering Applications of Artificial Intelligence*, 97, p. 104015. doi: 10.1016/j.engappai.2020.104015.

Zhou, X., Sun, J., Cui, P., Lu, Y., Lu, M. and Yu, Y. (2021b). A Fast and Robust Open-Switch Fault Diagnosis Method for Variable-Speed PMSM System. *IEEE Transactions on Power Electronics*, 36(3), pp. 2598–2610. doi: 10.1109/TPEL.2020.3013628.